Formulation of a new footprint model for measuring fluxes of biological resuspension

Uri Shavit[1], Nir Marom[1,2], Roi Holzman[2,3], Emmanuel Boss[4], Timor Katz[5] and Gitai Yahel[6]

[1]Civil and Environmental Engineering, Technion, Haifa, Israel
[2]The Inter-University Institute for Marine Sciences, POB 469, Eilat, 88103, Israel
[3]School of Zoology, Faculty of Life Sciences, Tel Aviv University, Tel Aviv, 69978, Israel
[4]School of Marine Sciences, University of Maine, Orono, ME 04469, USA
[5]Israel Oceanographic & Limnological Research, Tel Shikmona, 31080 Haifa, Israel
[6]The Faculty of Marine Sciences, Ruppin Academic Center, Michmoret, Israel

Abstract

Biological resuspension of sediments from the seafloor occurs when fish and other marine creatures search for food and shelter. In high-energy habitats, waves and currents dominate the resuspension of sediments, however, studies suggest that biological resuspension is the dominant process in areas below the wave action including the deep sea and in low energy zones such as lagoons and other sheltered basins. Biological resuspension is a highly punctuated process both in time and space, generating high concentration sediment plumes that quickly sink and disperse. It is therefore not surprising that despite its potentially large impact, no quantitative data exists regarding its extent and ecological impact in the ocean. To resolve the difficulty in monitoring and quantifying these short-live resuspension events, we develop a model named the *footprint model* that converts field measurements of horizontal sediment fluxes, into estimates of long-term average fluxes of biological resuspension. Measurements of the horizontal fluxes of the suspended sediments by off-the-shelf instruments serve as an input to the *footprint model*, which are then analyzed by the algebraic equations of the model. Given a horizontal velocity profile, the model quantifies the sedimentation of heavy particles as a function of their size, initial distribution and advection. Flow measurements are then used to include the effect of dispersion by the turbulent flow. The document provides a detailed description of the model derivation and proposes techniques that can be used for validation of the model results.

1.   Introduction

Resuspension of sediments from the sea floor can potentially control key sedimentary processes such as remineralization rates, silica dissolution, denitrification and the quality and burial rate of organic matter and hence carbon sequestration (Inthorn et al. 2006, Yahel et al. 2008, Katz et al. 2009). Resuspension also plays a major role in sediment transport which affects sediment erosion, sediment accumulation (Vidal 1994, Stahlberg et al. 2006, Teague et al. 2006) and the distribution of organisms such as bacteria and filter feeders (Cotner 2000, Snelgrove and Butman 1994). As opposed to the so called "physical resuspension" that is generated by strong currents and waves, biological resuspension occurs at the bottom of the sea due to the activity of marine creatures such as fish. It has been suggested that in biologically rich areas such as coral reefs, biological resuspension dominant over physical resuspension. In deep sea regions where currents and waves are negligible, biological activity (and to some extent gas bursts) are the most likely mechanisms that can generate sediment resuspension, and yet, there are surprisingly few biological resuspension studies, but, the ones that exist suggest an impact far greater than was previously suspected (Yahel et al., 2002, Yahel at al., 2008, Katz, et al., 2009, Katz et al., 2016).

The average flux of biological resuspension, $\bar{J}_z (kg\ m^{-2}s^{-1})$, is defined as the average mass of particles, resuspended vertically from the sea floor by biological activity, per unit time and unit floor area. It is positive upwards and by multiplying $\bar{J}_z$ over a given floor area and a given time period, we should be able to provide an estimate of the total mass of particles that is biologically resuspended. However, such an estimate is difficult to obtain. Biological resuspension is a highly punctuated process, both in time and space, arbitrarily generating plumes with high concentration of resuspended sediment that quickly sink and disperse (Yahel et al., 2008). It is therefore understood that measurements of concentration and velocity near the bottom are not likely to provide a representative estimate of $\bar{J}_z$ without an appropriate model. Imaging techniques must cover a wide enough floor area and are often limited under turbid conditions; Sediment traps at multiple heights may be attractive (Bloesch, 1994) but since they provide an integration over prolonged deployment time, it is difficult to separate the putative effect of biological resuspension from other factors (Gilboa et al., 2018).

As there are multiple sources of particles in the ocean, the only approach that can provide a direct estimation of $\bar{J}_z$ is a complete mass balance formulation. A mass balance calculation can be obtained by computational fluid dynamics (CFD) or by measuring the velocity and particle concentration around and inside local control volumes. However, while the former is not computationally feasible at ocean scales, the latter needs to fully cover the control volume faces and inner space by measurements and it is therefore unrealistic.

To overcome these limitations, we propose in this document a model for $\bar{J}_z$ that is based on measurements of concentration and velocity along a vertical profile within the lower section of the benthic nepheloid layer (BNL). Specifically, the model is designed to convert the measured horizontal flux of particles into an estimate of $\bar{J}_z$. The current document focuses on describing the derivation of the model and its formulation.

2.   Model derivation

We aim at estimating $\bar{J}_z$ by using a stationary sensor (or sensor array) that is located downstream from resuspension events and records simultaneously the particles velocity and concentration as a function of height above the seabed. Examples of off-the-shelf sensors include Acoustic Doppler Current Profilers (ADCP), vertical array of Acoustic Doppler velocimeters (ADVs), and Optical Backscatter Sensors (OBSs). Fig. 1 shows an image taken during a recent feasibility test in the Gulf of Aqaba. The release of the particles is demonstrated in a [side view](#) and a [top view video clips that](#) were taken during one of these tests. Velocity was measured by the ADCP and ADVs, concentration was obtained from data collected by the OBS, the back scattering of the ADVs (Fugate and Friedrichs, 2002) and by a submersible particle size analyzer (LISST 200x) which also provides particle size distributions.
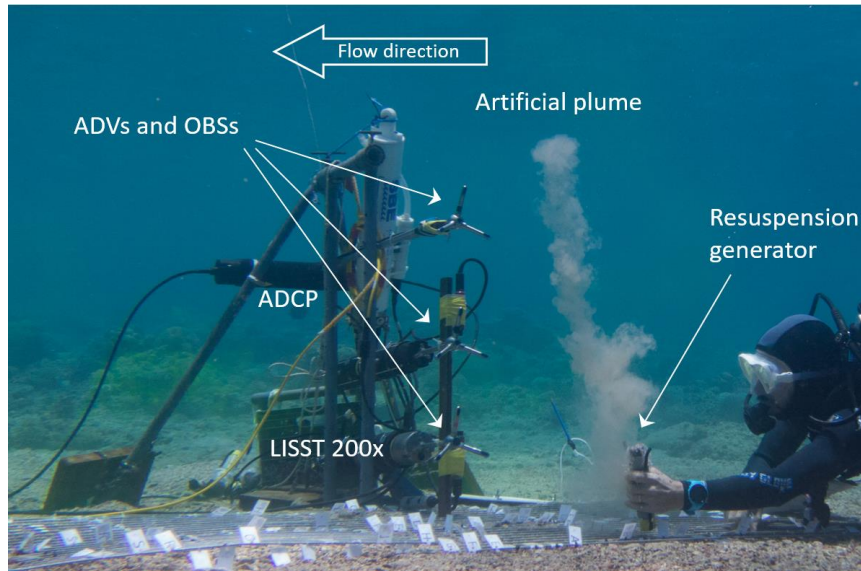

Fig. 1 An image taken during a feasibility test in the Gulf of Aqaba. The measurement rig consists of three ADVs, three OBS, a down looking 2 MHz ADCP, and a submersible laser-diffraction based particle size analyzer (LISST 200x). A diver is shown to release a known mass of sediment particles from a specially designed resuspension generator. A labelled grid was placed at the bottom to mark the location of each plume release. The instruments were cabled to the shore so that data could be visualized in real-time. The plume is detected in this image between the release location and the instruments. A remote release mechanism is being developed to replace the need for a diver. Two videos clips, [side view](#) and a [top view](#), were taken during one of these tests.

The model, named the *footprint model*, aims at converting the data collected by instruments such as those shown in Fig. 1, into an estimation of $\bar{J}_z$. The overbar in $\bar{J}_z$ states that we aim at estimating a long-time average flux and the subscript z is to state that $\bar{J}_z$ is a vertical flux that enters the control volume from its bottom. We assume that the vertical velocity of the particles during the resuspension event is significantly larger than the horizontal water velocity such that the horizontal advection during the initial resuspension event is negligible. Concurrent to the horizontal advection, we consider flow dependent turbulent dispersion and size (and potentially concentration) dependent settling. We apply a mass balance approach to convert the sensor data into an estimate of $\bar{J}_z$. We assume that the number of resuspension events, measured during the deployment time, is large enough to assume that they represent, on average, the variety of particle clouds that were generated upstream from the sensor, i.e., the number of events is large enough to use an analogy of a non-point (surface) source to represent, on average, multiple point-source events.

We define a control volume (Fig. 2) with dimensions that are defined by the lateral width of the sensor measurement volume, Δy_s, the maximum height h at which the resuspended particles reach the sensor and a length L, named the *footprint length* that is defined in the next sections for the case dominated by settling and for the case dominated by turbulent mixing. By measuring the concentration, $c(z,t)$, and the particle velocity, $\vec{u}_p(z,t) = (u_p, v_p, w_p)$ at the "sensor wall" as a function of height z and time t (Fig. 2), the flow rate of particles that exit the control volume, $\dot{m}_m$, is obtained by the following double integral,

$$\dot{m}_m = \frac{1}{T'} \int_t^{t+T'} \Delta y_s \int_0^h (c - c_b)(\vec{u}_p \cdot \hat{\imath}) dz \, dt' \tag{1}$$

where t' is an integration time which instead of being continuous, defines the time segments of a conditional sampling (Antonia, 1981 and Businger and Oncley, 1990) with an accumulated time T'. $\hat{\imath}$ is a unit vector in the x direction. The background concentration, c_b, can be identified by measurements taken during times of no resuspension events.

(a)   (b)
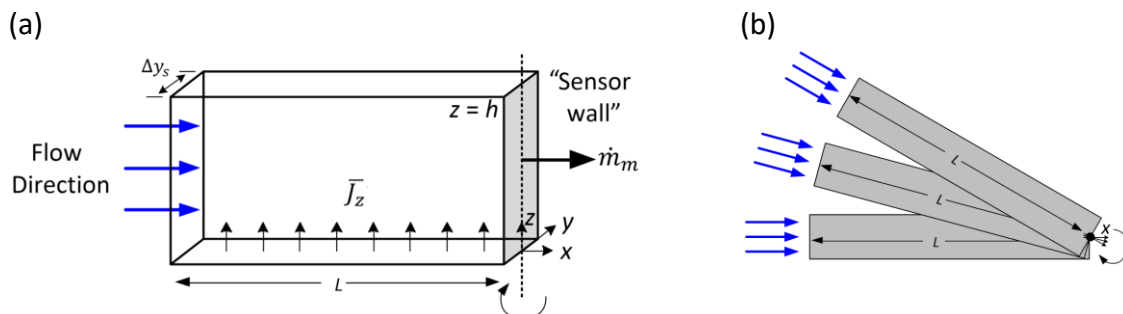

Fig. 2 (a) The control volume, and (b) a top view of the control volume aims at demonstrating that the control volume is rotating with the flow so that it is always oriented parallel to the flow direction with the sampling system located at its most downstream face.

In order to estimate $\bar{J}_z$ we define the flow rate of resuspended particles that enter the control volume from the ocean floor as $\dot{m}_r = \bar{J}_z \Delta y_s L$ and the ratio between $\dot{m}_m$ (the flow rate of particles that exit the control volume) and $\dot{m}_r$ as $\alpha = \dot{m}_m / \dot{m}_r$ such that,

$$\bar{J}_z = (\dot{m}_m)/(\alpha \Delta y_s L) \tag{2}$$

where $\Delta y_s L$ is the floor area of the control volume. Eq. 2 can be used to compute $\bar{J}_z$ only if α and the *footprint length*, L, are known. The calculation of L and α is derived by assuming that the dominant fluxes that contribute to the mass balance calculation are those that cross the sea floor and the 'sensor wall'. The justifications for this assumption are as follows: As illustrated in Fig. 2, the control volume is a narrow box that can rotate around a vertical axis such that its long horizontal axis is always aligned with the flow. As a result, particles do not cross its side walls by mean advection. The conditional sampling is required, for example, to assure that this assumption holds, which is achieved by ignoring data that was collected when the velocity magnitude was below a threshold value. The flux of particles that sinks from the water column and enter from above can be estimated by a variety of methods as described in Appendix A. These may include the use of particle size distribution (PSD) measurements, measurements of the mean vertical velocity $\overline{w}_p$, the use of sediment traps and the use of sediments cameras (Appendix A). Note, however, that particles that reach the bottom before reaching the 'sensor wall' do not contribute to $\dot{m}_m$ and have no impact on the calculation of $\bar{J}_z$.

The model assumes that the fluxes that cross the upstream side of the control volume contribute nothing to the mass balance calculation. The location of the upstream face is at $x = -L$, the *footprint length*, which is also used to calculate the size of the floor area from where particles are resuspended and later cross the 'sensor wall'. We adopted here the terminology of the meteorological community by using the terms *footprint model* and *footprint length,* suggesting that our attempt to trace back the floor region of resuspension is similar to using *footprint* modeling to analyze the signature measured by monitoring stations and trace back the flux sources (Schuepp, et al., 1990, Leclerc and Thurtell, 1990, Duman et al., 2015). We propose to model the *footprint length* by considering particle settling and turbulent dispersion, "whoever comes first", such that particles that cross the upstream side of the control volume are not accounted for by the mass balance calculation. The description of the *footprint length* estimates is therefore split into two parts; the calculation of L by considering particle settling and the calculation of L by considering the role of turbulence dispersion.

2.1 The footprint length due to settling

When only settling and advection are considered, L is calculated as the maximum horizontal distance traveled by a particle before reaching the ground. The trajectory of this particle, named the *defining trajectory* (Fig. 3), starts at $(x, z) = (-L, h_p)$ and ends at the base of the sensor, at $(x, z) = (0, 0)$. It is presented here for a given particle size but later calculated separately for each size group. The shape of the trajectory is a function of the plumes' height, h_p, the particle horizontal mean velocity, $\bar{u}_p(z)$, and the particle settling velocity, $w_s(z)$. The differential relationships $dz_p = w_s dt$ and $dx_p = \bar{u}_p dt$ is used to calculate the *defining trajectory*, $z_p = z_p(x_p)$, and the *footprint length, L*,

$$x_p = -L + \frac{1}{w_s} \int_{h_p}^{z_p} \bar{u}_p(z) dz \tag{3}$$

$$L = \frac{1}{w_s} \int_{h_p}^{0} \bar{u}_p(z) dz \tag{4}$$

Eqs. 3 and 4 were derived for a constant w_s (per particle size group), however both can be derived for any known function $w_s = w_s(z)$. The *defining trajectory* is illustrated in Fig. 3 for the artificial case of a linear velocity profile. It also demonstrates that the value of α is equal to the ratio between the mass of particles above the *defining trajectory* (gray area) and the mass of particles in the rectangular area Lh. The reason is that only particles that start their trajectory from the gray area will be detected by the sensor and particles that start their motion from below the *defining trajectory* will sink before reaching the sensor. Hence, once the *defining trajectory*, $z_p = z_p(x_p)$, is known, α is calculated as,

$$\alpha = \frac{1}{L} \int_{x=-L}^{x=0} \int_{z=z_p(x_p)}^{z=h_p} f(z) dz \, dx \tag{5}$$

where $f(z)$ is a probability density function of the vertical distribution of resuspended particles, when the plume was formed (see Appendix B for a detailed derivation of Eq. 5).

We assume that during the deployment period, several resuspension events take place near the sensor wall ($x = 0$) such that the distribution of the concentration inside the plume is measured by the sensor and their average result can be used to define $f(z)$ and h_p. For the case of a uniform probability density function, $f(z) = 1/h_p$, Eqs. 4 and 5 show that when the velocity is uniform ($u(z) = u_0$), $L = -hu_0/w_s$ and $\alpha = 1/2$. When the velocity varies linearly ($u(z) = u_0(z/h)$, Fig. 3), $L = -hu_0/2w_s$ and $\alpha = 1/3$. Analytical derivation for velocity profiles such as logarithmic profiles and numerical integrations can provide solutions to any measured velocity profiles.
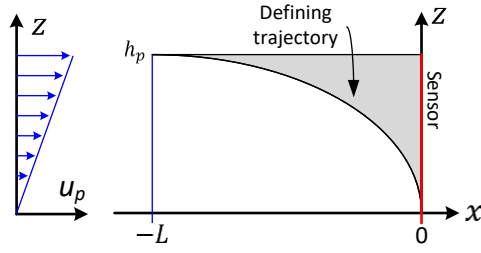
Fig. 3 The defining trajectory (black line) and the area representation of the coefficient α for the case of a linear velocity profile ($\alpha = \dot{m}_m/\dot{m}_r$, where $\dot{m}_m$ is represented by the gray area).
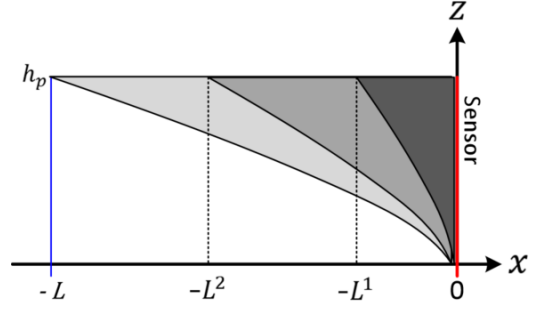
Fig. 4 The defining trajectory and the area representation for three particle size groups. L^i represents the maximal horizontal distance that a particle from size group i make.

Eqs. 4 and 5 were derived for the case of a mono size distribution. In order to expand the solution to the general case of particle size distribution, Eq. 5 is rewritten for a size group i, of a particle diameter d^i as,

$$\alpha^i = \frac{1}{L^i} \int_{x=-L^i}^{x=0} \int_{z=z_p^i(x_p^i)}^{z=h^i} f^i(z)dz\,dx \qquad (6)$$

from which $\alpha = \dot{m}_m/\dot{m}_r$ is obtained as follows,

$$\alpha = \sum_{i=1}^{n} \frac{r^i}{L} \int_{x=-L^i}^{x=0} \int_{z=z_p^i(x_p^i)}^{z=h^i} f^i(z)dz\,dx \qquad (7)$$

where r^i (the ratio $\dot{m}_r^i/\dot{m}_r$) and $f^i(z)$ are measured in the field during events that occur at the vicinity of the sensor, and L is calculated using Eq. 4 for the smallest size group. The effect of the particle diameter of the i-size group is demonstrated for three size groups in Fig. 4, showing the *defining trajectories* $z = z_p^i(x_p^i)$ and the corresponding *footprint length,* L^i for each size group.

2.2 The footprint length due to turbulent dispersion
When the effect of turbulent dispersion is considered, the *footprint length L* is defined by the distance it takes for the initial plume to disperse and approach the background ambient concentration, c_b. Under these conditions, a different formulation of L is needed. The dispersive flux is described by the correlation, $\overline{u_{p_i}'c'}$, where u_{p_i}' is the turbulent velocity in the i-direction and c' is the concentration fluctuation obtained by a proper signal filtering. We propose to estimate L by adopting a diffusion closure model, $\overline{u_{p_i}'c'} = -E_{ij}(\partial\bar{c}/\partial x_j)$, where the turbulent diffusion coefficient, E_{ij}, is estimated by the flow field. When using the

$E_{xz} \cong -\overline{u'w'}/(\partial \overline{u}/\partial z)$, we assume that the turbulent Schmidt number is ~unity and the velocity vertical gradient is main source of turbulence. The calculation of E_{xz} is straight forward and requires ensemble averaging which can be obtained with sampling rates lower than the turbulence frequencies. While longitudinal dispersion is expected to dominant the dilution process, E_{xz} is used to estimate the vertical mixing. As an alternative we consider using the measured turbulent kinetic energy ($k = 0.5u_i'u_i'$), an estimation of the dissipation rate (ε), and the measured Reynolds stress tensor ($\overline{u_i'u_j'}$) to calculate the components of the E_{ij} tensor (e.g., Argyropoulos and Markatos, 2015, Eq. 62),

$$E_{ij} \cong C_s \frac{k}{\varepsilon} \overline{u_i'u_j'} \tag{8}$$

where $C_s = 0.18 - 0.25$ (e.g., Kang and Choi, 2008, Eq. 4, Hanjalic, 1994, Eq. 5) and ε, the dissipation rate, is estimated using the inertial subrange dissipation method (Bluteau et al. 2011). While the implementation of Eq. 8 requires high frequency sampling, it is advantageous since it provides anisotropy information. This is an important advantage as we expect that E_{xx} will be the largest component and $\overline{u_{p_x}'c'}$ will contribute the most to the dilution of the resuspended plumes.

In order to estimate L we propose to follow an analytical solution of the advective diffusion Eulerian equation derived for the spread of an instantaneous truncated line source in an anisotropic turbulent flow (Socolofsky and Jirka, 2005, p. 147). By applying the only-time-dependent part of the solution, we estimate the *footprint length*, L, as,

$$L \cong \frac{m'\overline{u}_p}{4\pi c_b \sqrt{E_{xx}E_{yy}}} \tag{9}$$

where E_{xx} and E_{yy} are obtained, for example, by Eq. 8. The analytical solution is an approximation since it was derived for homogeneous turbulence. In addition, the time-dependent part of the line source solution that was used here (Eq. 9) ignores the dispersion in the vertical direction. As an alternative we propose to use a solution of an instantaneous point source (Socolofsky and Jirka, 2005, p. 145) from which we obtain the following estimate,

$$L \cong \frac{\overline{u}_p}{4\pi} \left(\frac{c_m V_s}{c_b \sqrt{E_{xx}E_{yy}E_{zz}}} \right)^{2/3} \tag{10}$$

where c_m represents the initial plume concentration and V_s is the sensor volume.

These estimates of the *footprint length* serve as a measure of the dominant process, namely gravitational sinking versus turbulent dispersion. When L of Eq. 4 is smaller than L of Eqs. 9-

10, the dominant process is sinking and vice versa. When sinking is dominant, Eq. 4 will be used and when turbulent dispersion is dominant Eqs. 9 or 10 will be used (with $\alpha = 1$). When the time scales of the two processes are of the same order of magnitude, a similar L value is expected to result from the two approaches. In such cases, a weighted value of α will be applied.

3.   Lagrangian stochastic resuspension simulator

It is proposed to test the *footprint model*, its assumptions and limitations by generating computerized resuspension events using particle tracking simulations. Plumes will be generated by assigning x, y, z random locations of n_p particles ($\approx 100,000$) using a Bivariate normal distribution in the x and y directions (Kotz et al., 2000). Each particle will be assigned a diameter d and a height z according to probability density functions, $f(d)$ and $f^i(z)$, that are defined for each size group i obtained from the sediment particle size distribution. Plumes will be released from the virtual ocean floor at random locations and random times using uniform distributions, and their individual particles will be advected, sink and disperse. The advective horizontal velocity of the particles, $\bar{u}_p(z)$, will be height dependent but uniform in the horizontal plane. Sinking (w_s) will follow Stokes terminal velocity using empirical adjustments proposed by Dietrich (1982) and optionally modified as a function of concentration using the empirical formula of Richardson and Zaki (1954) with the exponent n proposed by Cheng (1997) and by Baldocka et al. (2004). Dispersion will be obtained by using a random walk generator determined by the turbulent properties of the flow. The simplest approach would be to generate an eddy velocity $u_i' = N_G u_{i,rms}'$ (Guha, 2008) and add it to the mean velocity ($\bar{u}_p, 0, w_s$) while keeping the eddy life-time around twice the measured integral time scale. We use $u_{i,rms}'$ as the root mean square velocity in the i direction and N_G as a random number sampled from a Gaussian distribution with zero mean and unity standard deviation. An alternative, more complex approach would be to follow Thomson (1987) and apply the Langevin equation (see, for example, Duman et al., 2015).

To relate the computerized simulation to the output of commercially available sensors that can be deployed near the ocean floor, the particle tracking code will include acoustical and optical modules (see appendix C). This approach will allow us to simulate the expected signal that will be obtained by instruments such as ADCP, ADV, LISST and OBS positioned at designated heights above the bottom. These modules will translate information from the simulated distribution of particles (concentration, size, shape, composition) into the expected signal of the simulated instruments. Particle composition and the instrument wavelength (or frequency) determine the contrast in the speed of light (or sound) with the environment. This contrast along with particle size are the primary determinants of the scattering intensity and angular pattern of a given particle (the efficiency factor of a given

optical property or target strength for acoustic backscattering). Integrating over the suspension at a given point and time (concentration, size, composition) provides the likely signal that will be recorded by an instrument measuring the given optical or acoustical property there. While assumptions must be made (e.g. spherical shape for particles), this problem is well posed and can be used to better link the actual instrument signal and the estimate of $\bar{J}_z$ with the benefit of adding the effect of potential bias and random noise sources.
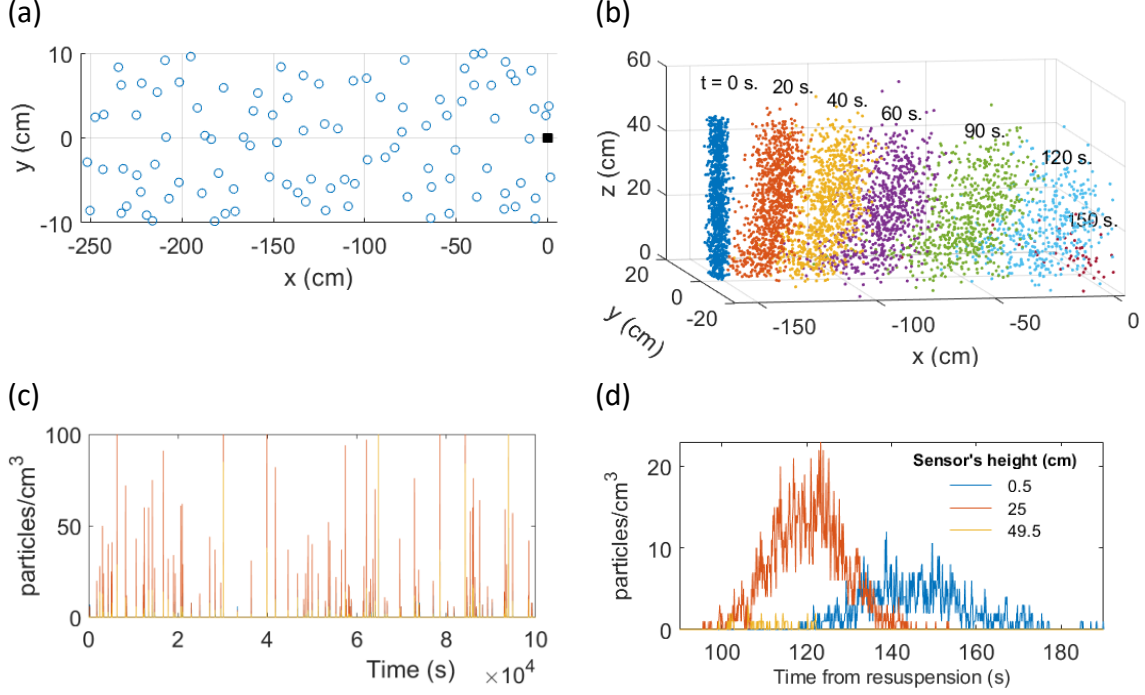

Fig. 5 Preliminary results of the Lagrangian stochastic simulation. (a) The locations from where plumes were released (blue circles). The sensor location is marked by a black square; (b) Snapshots of a plume at seven different times ($t = 0 - 150s$) while moving in a logarithmic boundary layer $(u(z) = \frac{u^*}{\kappa} \log \left(\frac{z-\delta}{z_0}\right)$, $\delta = 0.2 \; cm$ and $z_0 = 0.2 \; cm$), sinking at $w_s = -0.2 \; cm \; s^{-1}$, and spread at $E = 0.4 \; cm^2 s^{-1}$ (only 1000 particles of the 10^6 computed are shown); (c) Concentration measured by three simulated sensors, located at $z = 0.5, 25$ and $49.5 \; cm$, generated by the release of 100 plumes; (d) Zoom-in example of the results from Fig. 5c.

An early version of the simulation code was developed using the parallel capabilities of MATLAB. It was found that by sophisticated sampling we can run hundreds of complete simulations in less than 24 hours on a multi-core workstation. The simulation plan will start with code testing and sensitivity analysis of simulation parameters such as time step, number of plumes and number of plume particles needed to generate a representative and repeatable result. Then, the simulated concentration profile, $c(z, t)$, will be obtained by counting the number of particles that are in the sensor volume at any given time. The ability of the *footprint model* to calculate $\bar{J}_z$ and reconstruct the imposed flux J_i will be evaluated by presenting the error $(\bar{J}_z/J_i - 1)$ as a function a large variety of the problem variables.

These will include current velocities, particle size distributions, turbulence, the potential role of surface waves, time duration of the deployment, the sensor sampling frequency and measurement volume, degree of plumes overlap, level of plume nonuniformities of their height, width, shape and length of generation, and instrumentation inaccuracies. The simulations results will provide a quantitative assessment of the accuracy and limitations of the *footprint model* and its ability to estimate fluxes of biological resuspension.

4.   Developing the H2VTool

Once data is collected in the field, an estimation of $\overline{J}_z$ can be obtained. It requires first signal filtering followed by a set of decisions that involves the use of Eqs. 4, 7, 8 and 9 or 10. The input to these equations involves data extracted from resuspension events that took place near the sensor, information about particle sizing and a statistical assessment for the accuracy of the result. For the future users of the *footprint model*, a MATLAB tool, named *H2VTool*, will be developed. Data collected by the sensors and inputs provided by the user through a graphical user interface (GUI) will generate estimated values of the fluxes of biological resuspension.

5.   Signal filtering

Prior to applying the *footprint model*, the signal obtained at the "sensor wall" will be filtered in order to isolate the biological events from other sources such as variations in the upstream concentration field and instrumentation noise. In addition to spectrum-based filters, fast Fourier transform, and orthonormal wavelet transform, we tested a series of filters developed by the hydrological scientific community. We found that time series collected in monitoring stations of rivers and estuaries are very similar to the signal generated by biological resuspension events. We therefore adopt a variety of hydrological algorithms derived for the separation of base flows flow from flood events in flow (Lott and Stewart, 2016), often named 'hydrograph separation'. An example of spectral filtering of sediment resuspension events at 4,800m depth is presented in Pak (1983). While the author did not suspect biological resuspension to take place, and left the cause of these events as unknown, the 'signature' of the high frequency events filtered with spectral analysis is similar to the signal we observe in shallow areas due to fish (e.g., Fig 6a in Yahel et al. 2008).

References

Antonia, R.A., 1981. Conditional sampling in turbulence measurement. Annual Review of Fluid Mechanics, 13: 131-156.

Argyropoulos, C.D., and Markatos N.C., 2015. Review: Recent advances on the numerical modelling of turbulent flows. Applied Mathematical Modelling, 39: 693–732.

Baldocka, T.E., Tomkinsa, M.R., Nielsena, P., and Hughes, M.G., 2004. Settling velocity of sediments at high concentrations. Coastal Engineering, 51: 91–100.

Bloesch, J., 1994. A review of methods used to measure sediment resuspension. Hydrobiologia, 284(1): 13–18.

Bluteau, C.E., Jones, N.L., and Ivey, G.N., 2011. Estimating turbulent kinetic energy dissipation using the inertial subrange method in environmental flows. Limnology and Oceanography: Methods, 9: 302–321.

Businger, J.A. and Oncley, S.P., 1990. Flux measurement with conditional sampling. Journal of Atmospheric and Oceanic Technology, 7(2): 349-352.

Cheng, N.S., 1997. Effect of concentration on settling velocity of sediment particles. Journal of Hydraulic Engineering, 123(8): 728-731.

Cotner, J.B., 2000. Intense winter heterotrophic production stimulated by benthic resuspension. Limnology and Oceanography, 45: 1672–1676.

Dietrich, W.E., 1982. Settling velocity of natural particles. Water Resources Research, 18(6): 1615-1626.

Duman, T., Tanny, J., Dicken, U., Siqueira M.B., and Katul, G.G., 2015. Footprint estimation for multi-layered sources and sinks inside canopies in open and protected environments. Boundary-Layer Meteorology, 155: 229-248.

Fugate, D.C., and Friedrichs, C.T., 2002. Determining concentration and fall velocity of estuarine particle populations using ADV, OBS and LISST. Continental Shelf Research, 22: 1867–1886.

Gilboa, M., Katz, T., Shavit, U., Grosbard, S., Torfstien, A., and Yahel, G., 2018. Novel approach to measure the rate of sediment resuspension at the ocean and to estimate the contribution of fish activity to this process. Particles in Europe, PiE-2018, 14-17 October 2018, Lisbon, Portugal, page 57. http://www.sequoiasci.com/wp-content/uploads/2019/11/Proceedings-of-PiE-2018.pdf,

Guha A, 2008. Transport and deposition of particles in turbulent and laminar flow. Annual Review of Fluid Mechanics, 40: 311–341.

Hanjalic, K., 1994. Review: Advanced turbulence closure models a view of current status and future prospects. International Journal of Heat and Fluid Flow, 15(3): 178-203.

Inthorn, M., Wagner, T., Scheeder, G., and Zabel, M., 2006. Lateral transport controls distribution, quality and burial of organic matter along continental slopes in high-productivity areas. Geology, 34(3): 205-208.

Kang, H. and Choi, S., 2008. Turbulence modeling of solute transport in open-channel flows over submerged vegetation. Advances in Water Resources and Hydraulic Engineering - Proceedings of 16th IAHR-APD Congress and 3rd Symposium of IAHR-ISHS. Berlin, Heidelberg: Springer, pp. 674-679.

Katz, T., Yahel, G., Tunnicliffe, V., Herut, B., Whitney, F., Snelgrove, P.V.R., and Lazar, B., 2016. The silica cycle in a Northeast Pacific fjord; the role of biological resuspension. Progress in Oceanography, 147: 10–21.

Katz, T., Yahel, G., Yahel, R., Tunnicliffe, V., Herut, B., Snelgrove, P., and Lazar, B., 2009. Groundfish overfishing, diatom decline, and the marine silica cycle: Lessons from Saanich Inlet, Canada, and the Baltic Sea cod crash. Global Biogeochemical Cycles, 23(4): GB4032, doi:10.1029/2008GB003416.

Kotz, S., Balakrishnan, N., and Johnson, N. L., 2000. Bivariate and trivariate normal distributions. Ch. 46 in Continuous Multivariate Distributions, Vol. 1: Models and Applications, 2nd ed. New York: Wiley, pp. 251-348.

Leclerc, M.Y., and Thurtell, G.W., 1990. Footprint prediction of scalar fluxes using a Markovian analysis. Boundary-Layer Meteorology, 52(3): 247-258.

Lott, D.A. and Stewart, M.T., 2016. Base flow separation: A comparison of analytical and mass balance methods. Journal of Hydrology, 535: 525-533.

Pak, H., 1983. Fluctuations of beam-attenuation coefficient in the lowest 2m on the continental rise off Nova Scotia. Marine Geology, 51: 77-97.

Richardson, J.F., and Zaki, W.N., 1954. Sedimentation and fluidisation: part 1. Transactions of the Institution of Chemical Engineers, 32: 35-53.

Schuepp, P.H., Leclerc, M.Y., MacPherson, J.I., and Desjardins, R.L., 1990. Footprint prediction of scalar fluxes from analytical solutions of the diffusion equation. Boundary-Layer Meteorology, 50(1-4): 355-373.

Snelgrove, P.V.R. and Butman, C., 1994. Animal-sediment relationships revisited: cause versus effect. Oceanography and Marine Biology: An Annual Review, 32: 111–177.

Socolofsky, S.A., and Jirka, G.H., 2005. Special topics in mixing and transport processes in the environment. Engineering - Lectures, 5th Edition, Coastal and Ocean Engineering Division, Texas A&M University, pp. 1-93.

Stahlberg, C., Bastviken, D., Svensson, B.H. and Rahm, L., 2006. Mineralisation of organic matter in coastal sediments at different frequency and duration of resuspension. Estuarine, Coastal and Shelf Science, 70: 317–325.

Teague, W.J., Jarosz, E., Keen, T.R., Wang, D.W., and Hulbert, M.S., 2006. Bottom scour observed under Hurricane Ivan. Geophysical Research Letters, 33, L07607, doi:10.1029/2005GL025281 .

Thomson, D., 1987. Criteria for the selection of stochastic models of particle trajectories in turbulent flows. Journal of Fluid Mechanics, 180: 529–556.

Vidal, M., 1994, Phosphate dynamics tied to sediment disturbances in Alfacs Bay (NW Mediterranean). Marine Ecology Progress Series, 110:211–221.

Yahel, R., Yahel, G. and Genin, A., 2002. Daily cycles of suspended sand at coral reefs: A biological control. Limnology and Oceanography, 47: 1071–1083.

Yahel, G., Yahel, R., Katz, T., Lazar, B., Herut, B. and Tunnicliffe, V., 2008. Fish activity: a major mechanism for sediment resuspension and organic matter remineralization in coastal marine sediments. Marine Ecology Progress Series, 372: 195–209.

Appendices

Appendix A – Alternative measurement methods

Alternative measurement methods are needed in order to test the model, validate its results and identify its limitation. In addition, identifying the potential contribution of particles that sink from above, enter the control volume and leave it through the "sensor wall" is required in order to exclude this flux from the mass balance calculation. Four potential methods are described.

A1. Particle sizing

Particle size distributions, that are collected above the BNL by a submersible particle size analyzer (e.g., LISST 200X, Sequoia), can be used to estimate the flux of particles that sink from above. This is obtained by assuming that the sinking velocity, w_s, is known for given particle size and concentrations. Note, that while w_p (Appendix A1) is the measured vertical velocity of the particles, w_s is calculated using the measured particle size and concentration. Stokes terminal velocity is calculated using empirical adjustments proposed by Dietrich (1982) and optionally modified as a function of concentration using the empirical formula of

Richardson and Zaki (1954) with the exponent n proposed by Cheng (1997) and by Baldocka et al. (2004). Assume that the size distribution of the particles is given by N size groups and that the flux of particles that sink from above of each size group, i, is $\bar{J}_{a,i}$, an estimate of $\bar{J}_a$ is obtained as follows,

$$\bar{J}_a = \sum_{i=1}^{N} \bar{J}_{a,i} = \sum_{i=1}^{N} c^i w_s^i \tag{A1}$$

where c^i is the concentration of the ith size group and w_s^i is its sinking speed.

If a second submersible particle size analyzer is positioned within the BNL, a similar form of Eq. A1 can be used to estimate the resuspension fluxes themselves. Since the trajectory of each resuspended particle consists of an upward motion followed by a sinking motion, only sinking (negative w) velocities will be included in the calculations. Since all particles will eventually sink back to the floor, and since the maximum height where resuspended particles can reach is size dependent, an estimate of $\bar{J}_z$ should be obtained at the lowest point that is not contaminated by the floor itself. This is where the downward flux will be consisted of almost all the size groups and will, therefore, be the highest. In order to identify this vertical location, it is proposed to install the near bottom LISST on a micro profiler that will continuously scans the first two meters above the seafloor at a two cm-scale resolution. Once the vertical location of the maximum downward flux is identified (z_m), the resuspension flux will be estimated as follows,

$$\bar{J}_z = \sum_{i=1}^{N} c^i(z_m) w_s^i(z_m) - \bar{J}_a \tag{A2}$$

A2. The defining trajectory method
The result obtained by Eq. A1 can be validated by using a slight modification of Eq. 1 as follows,

$$\dot{m}_a = \frac{1}{T''} \int_t^{t+T''} \Delta y_s \int_0^h (c - c_b)(\vec{u}_p \cdot \hat{\imath}) dz \, dt' \tag{A3}$$

where T' was replaced by T''. The justification of using Eq. A3 is demonstrated in Fig. A1 for the case of a linear velocity profile. Particles that cross the top boundary are advected within the gray area and then exit the control volume through the sensor wall. Once The $\dot{m}_a$ is obtained, the flux is calculated by,

$$\bar{J}_a = \frac{\dot{m}_a}{L \Delta y_s} \tag{A4}$$

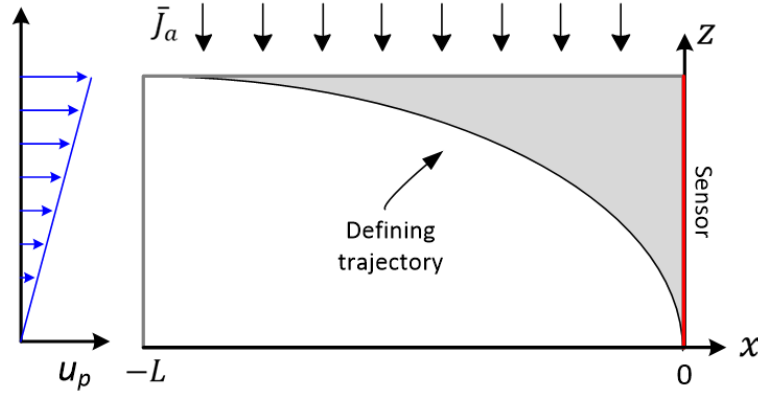where L is calculated using Eqs. 4 or B4.

Fig. A1 An illustration of the time periods during which the only flux that enters the control volume is settling of particles from the water column for the case of a linear velocity profile. Particles that cross the top boundary are advected within the gray area before exit the control volume through the sensor wall.

A3. Sediments traps

Direct measurements of the settling flux are obtained by deploying two pairs of sediment traps at 0.5 and 1 meter above the seabed and a third trap pair is moored above the benthic nepheloid layer, BNL (as suggested by Bloesch 1994). The downward flux, $\bar{J}_a$, is measured by the upper trap and the difference (in $g\ m^{-2}day^{-1}$) between the average rate obtained by the near bottom traps and the traps moored above the BNL is a direct estimator of the total resuspension rate at the measured height. To prevent contamination with sediments that might resuspend during the deployment, the near-bottom traps are deployed with elastic caps that are removed remotely by a time-release mechanism (Gilboa et al. 2018), or carefully by SCUBA divers.

A4. Direct measurement

The method assumes that the signal analysis tools, developed and tested here, can identify the times, T'', during which the only flux that enters the control volume is the settling of particles from the water column. The measurements published by Yahel et al. (2002) indicate that the night hours in a coral reef environment can serve as an example of such almost zero biological resuspension. As illustrated in Fig. A1, this settling flux, $\bar{J}_a$, is assumed uniform along the control volume top boundary and can be obtained by directly measuring the mean concentration $\bar{c}$ and the mean vertical velocity $\bar{w}_p$ at the highest measurement point of the sensor ($z = h$),

$$\bar{J}_a = \bar{c}(z = h)\ \bar{w}_p(z = h) \tag{A5}$$

A negative $\bar{w}_p(z = h)$ value will indicate that indeed $\bar{J}$ is a settling flux.

Appendix B – The derivation of α for the settling dominated regime

The ratio $\alpha = \dot{m}_m/\dot{m}_r$ is needed when estimating the flux $\bar{J}_z = (\dot{m}_m)/(\alpha \Delta y_s L)$. Here we describe the derivation of α for the settling dominated regime while considering a known (measured) particle size distribution (PSD). Assume that the size distribution of the particles is given by N size groups and that the resuspended flow rate of each size group, i, is $\dot{m}_{r,i}$. Similarly, the measured flow rate of each size group is $\dot{m}_{m,i}$ and we therefore define $\dot{m}_m$ and $\dot{m}_r$ as,

$$\dot{m}_r = \sum_{i=1}^{N} \dot{m}_{r,i} \quad \text{and} \quad \dot{m}_m = \sum_{i=1}^{N} \dot{m}_{m,i} \tag{B1}$$

Using the resuspension flow rate of all size groups combined, $\dot{m}_r$, the relative contribution of group i is $r_i = \dot{m}_{r,i}/\dot{m}_r$ and α can be written as,

$$\alpha = \frac{\dot{m}_m}{\dot{m}_r} = \frac{\sum_{i=1}^{N} \dot{m}_{m,i}}{\dot{m}_r} = \frac{\dot{m}_{m,1}\, r_1}{\dot{m}_{r,1}} + \frac{\dot{m}_{m,2}\, r_2}{\dot{m}_{r,2}} + \cdots = \sum_{i=1}^{N} \frac{r_i \dot{m}_{m,i}}{\dot{m}_{r,i}} \tag{B2}$$

Since $1/\dot{m}_r = r_i/\dot{m}_{r,i}$ for any i-group. While $\dot{m}_{m,i}$ are measured, r_i and $\dot{m}_{r,i}$ are unknowns and therefore an expression for α must be derived. We start with rewriting Eq. 3 for each size group i,

$$x_p^i = -L^i + \frac{1}{w_s^i} \int_{h_p^i}^{z_p^i} \bar{u}_p(z)dz \tag{B3}$$

from which the *defining trajectory*, $z_p^i = z_p^i(x_p^i)$, is obtained for each size group. By substituting $x_p^i = 0$ and $z_p^i = 0$, we derive the *footprint length*, L^i, of each group,

$$L^i = \frac{1}{w_s^i} \int_{h_p^i}^{0} \bar{u}_p(z)dz \tag{B4}$$

Particles from size group i that were resuspended at a distance larger than L^i upstream from the sensor will sink to the floor before reaching the sensor and therefore not measured. While the highest starting point h_p^i and the settling velocity w_s^i are size dependent, the horizontal mean velocity $\bar{u}_p$ is assumed to be the same for all groups. Note the important distinction between L and L^i; while L^i represents the *footprint length* of size group i, L is calculated by Eq. B4 for the smallest particle size group.

The initial distribution of the resuspended particles defines the locations from which each particle begins its trajectory. This initial distribution of particles, in the space above the sea

floor, is represented by a pseudo source term, $S^i(x, y, z)$, that is a function of the resuspension rate, $\dot{m}_{r,i}$, and the density probability function of the initial distribution along the vertical axis for each group size, $f^i(z)$,

$$S^i(x, y, z) = \frac{\dot{m}_{r,i}}{\Delta y_s L} f^i(z) \tag{B5}$$

The measured mass that crosses the "sensor wall" per time, $\dot{m}_{m,i}$, is obtained by integrating S^i over the volume confined above the *defining trajectory* (the gray area in Fig. 3),

$$\dot{m}_{m,i} = \int_{x=-L^i}^{0} \int_{z=z_p^i(x_p^i)}^{h_p^i} \int_{-\Delta y_s/2}^{\Delta y_s/2} S^i(x, y, z) \, dy \, dz \, dx \tag{B6}$$

Note that in B5 we used L and in B6 we used L_i. The *footprint length*, L, is defined by the longest horizontal distance, L_i, such that it accounts for all the particles, from all size groups. This is the reason L is calculated by Eq. B4 for the smallest particle size group. Since particles, even from the smallest size group, that were resuspended from $x < -L$ sink to the floor before reaching the sensor, the calculation of the resuspended mass, $\dot{m}_{r,i}$, is calculated using L (Eq. B5). However, the mass of each group size that reach the sensor, originates from locations above the individual *defining trajectory* of that group size, and therefore the integration interval in B6 is defined by L^i. Note that except for the smallest particles, integrating along x from $-L$ to $-L_i$ has zero contribution.

Plugging Eq. B5 in Eq. B6 results in,

$$\frac{\dot{m}_{m,i}}{\dot{m}_{r,i}} = \frac{1}{L} \int_{x=-L^i}^{0} \int_{z=z_p^i(x_p^i)}^{h_p^i} f^i(z) \, dz dx \tag{B7}$$

and finally, plugging Eq. B7 into Eq. B2 result in an estimate for α,

$$\alpha = \frac{\dot{m}_m}{\dot{m}_r} = \sum_{i=1}^{N} \frac{r_i}{L} \int_{x=-L^i}^{0} \int_{z=z_p^i(x_p^i)}^{h_p^i} f^i(z) \, dz dx \tag{B8}$$

which is identical to Eq. 7 above.

Finally, it is interesting to note that there is strong link between $f(z)$ (Eq. 5) and the time integral of the concentration at each height z of the sensor, $c(z, t)$. With some additional derivation this linkage can be used to obtain $f(z)$ in the field. This method can potentially replace the suggestion to measure $f(z)$ during events that occur at the vicinity of the sensor. It is based on the understanding that in a pure settling case of a uniform particle size

distribution, each settling trajectory (e.g., the defining trajectory) is crossing the sensor at a different height. As a result, $f(z)$ is scaled with the time integral of the mass that crosses the sensor wall at each z during the time of deployment. The upper most trajectory samples the upper water layer while lower trajectories sample an increasing depth of water and the integration of $f(z)$ from any given z to h (the top of the control volume) is equal to the time integral of $c(z,t)$ during the time of deployment T at the same height z.

Appendix C – converting particle concentrations to measured optical and acoustical properties

C1. Optics
Given a particle size, index of refraction (that is the ratio of light speed within the particle relative to that in the medium), absorption (often described as an imaginary part of the index of refraction) and wavelength of light, the optical properties of the said particle (e.g. angular scattering, absorption coefficient, attenuation coefficient), if spherical, can be computed to the desired accuracy (Bohren and Huffman, 1983). Models also exists for more complex shapes (e.g. Mishchenko et al., 2000). Sediment particles in the marine environment are dominated by inorganic material and thus have a relatively high index of refraction (compared to organic particles) which means that their absorption can be ignored, particularly in the red and IR wavelengths used by the proposed submersible particle size analyzer (LISST 200X, Sequoia) and Optical Backscatter Sensor (OBS).

For a population of particles (the differential size distribution denoted as $N(D)$, in units of number of particles per volume per length, with D as the particle diameter) of uniform composition (hence uniform index of refraction, n) the attenuation coefficient of the LISST (c_p) can be computed from:

$$c_p(\lambda = 670nm) = \frac{\pi}{6} \int_{D_{min}}^{D_{max}} N(D)Q_c(D,n)D^2 dD \tag{C1}$$

where $Q_c(D,n)$ is the attenuation efficiency factor computed from a Mie code (e.g. Bohren and Huffman, 1983). Angular scattering, as measured by the LISST in the forward direction and the OBS in the back direction are computed as follows:

$$\beta_p(\lambda,\theta) = \frac{\pi}{6} \int_{D_{min}}^{D_{max}} \int_{0}^{\pi} W(\theta)N(D)S_{11}(\theta)Q_b(D,n)D^2 dD d\theta \tag{C2}$$

where $W(\theta)$ is the instrument angular weighing function (a property of the instrument), $Q_b(D,n)$ is the scattering efficiency factor and $S_{11}(\theta)$ is the first element of the Mueller

matrix, both outputs of the Mie code. The same framework can also be extended to model aggregates (Boss et al., 2009).

C2. Acoustics

The mean (root-mean-squared) backscattered pressure ($\langle P_b \rangle$) from a suspension of scatterers for a given frequency of sound can be written as (Downing et al., 1995):

$$\langle P_b \rangle = k_s k_t \sqrt{M} e^{-2\alpha r} \tag{C3}$$

where k_t is an instrument constant, M is the square root of the particle mass concentration, k_s is a parameter describing the acoustical properties of the scatterers (hence sensitive to size and composition) and α is the mean attenuation coefficient between the sensor and the sample volume (their distance is denoted by r). The attenuation can further be decomposed to that due to water (α_w, a function of temperature end salinity) and that of the particles ($\alpha_p = \alpha^* M$, where α^* is the specific attenuation of the suspension, which can be determined theoretically given the particle size distribution and composition (just like with Mie theory for optics). From Thorne et al., (1991):

$$k_s = \frac{1}{\sqrt{\rho_s}} \sqrt{\frac{\langle a_s^2 |f(a_s, \theta)|^2 \rangle}{\langle a_s^3 \rangle}} \tag{C4}$$

where ρ_s is the particles density, a_s the particle's radius, $f(a_s, \theta)$ a form function (reflectivity factor) which can be computed using a variety of methods, and $\langle a_s^3 \rangle$ is an average over the size distribution. The specific attenuation itself can be computed using (e.g. Medwin and Clay, 1998):

$$\alpha^* = \frac{3\sigma_t}{4\pi\rho_s \langle a_s^3 \rangle} \tag{C5}$$

where the acoustic cross section, σ_t, is computed from:

$$\sigma_t = \frac{\pi \langle a_s^2 \rangle}{2} \int_0^\pi |f(a_s, \theta)|^2 sin\theta d\theta \tag{C6}$$

Since the instruments measure acoustic intensity, we write it in that form (Medwin and Clay, 1998):

$$I = \frac{\langle P_b \rangle^2}{\rho c} \tag{C7}$$

where ρc is the product of the water density and the speed of sound.

Acoustical instruments use logarithmic detectors, hence, to compute intensity from counts we need to convert the counts as follows (Russo and Boss, 2012):

$$\frac{I_S}{I_0} = 10^{A \times counts/10} - 10^{A \times counts_{background}/10} \tag{C8}$$

where I_0 is a reference intensity (constant), A is the manufacturer conversion factor (dB/counts), $counts$ are the instrument reading, and $counts_{background}$ are the instrument reading in the clearest water (e.g. instrument blank).

From the above we expect that for a given particle size and composition the acoustic intensity will be proportional to SPM. However, as this proportionality constant will be size and composition dependent and hence will likely to vary with depth for a given sediment profile. Using existing theoretical framework to compute $f(a_s, \theta)$ (e.g. Thorne and Manley, 1993) we will convert the model output to profiles of acoustical properties which are likely to be recorded for a given acoustical instrument.

References

Bohren, C. F., and D. Huffman, 1987. Absorption and Scattering of Light by Small Particles. New York: Wiley, 530 pp .

Boss, E., Slade, W.H., and P. Hill, 2009. Effect of particulate aggregation in aquatic environments on the beam attenuation and its utility as a proxy for particulate mass. Optics Express, Vol. 17, No. 11: 9408-9420.

Downing, A., Thorne, P.D. and Vincent, C.E., 1995. Backscattering from a suspension in the near field of a piston transducer. The Journal of the Acoustical Society of America, 97(3):1614-1620.

Medwin, H., and C. Clay, 1998. Fundamentals of Acoustical Oceanography. Boston: Academic Press, 281 pp.

Mishchenko, M.I., Hoovenier, J.W. and Travis, L.D. (eds). 2000. Light Scattering by Nonspherical Particles: Theory, Measurements, and Applications. San Diego, California: Academic Press, 690 pp.

Russo, C.R. and E.S. Boss, 2012. An evaluation of acoustic doppler velocimeters as sensors to obtain the concentration of suspended mass in water. Journal of Atmospheric and Oceanic Technology, 29: 755-761.

Thorne, P., C. Vincent, P. Hardcastle, S. Rehman, and N. Peterson, 1991. Measuring suspended sediment concentrations using acoustic backscatter devices. Marine Geology, 98: 7–16.

Thorne, P., and J. B. C. Manley, 1993. Measurements of the form function and total scattering cross section for a suspension of spheres. Journal of the Acoustical Society of America, 93: 243–248.